

Supplementary Materials

**Iron-Doped Titanium Dioxide Hollow Nanospheres for Efficient Nitrogen Fixation and Zn-N<sub>2</sub> Aqueous Battery**

Xian-Wei Lv,<sup>a</sup> Xiao-Lu Liu,<sup>b</sup> Li-Jiao Gao,<sup>a</sup> Yu-Ping Liu,<sup>b</sup> Zhong-Yong Yuan,<sup>\*a,b</sup>

<sup>a</sup> National Institute for Advanced Materials, School of Materials Science and Engineering, Nankai University, Tianjin 300350, China.

<sup>b</sup> Key Laboratory of Advanced Energy Materials Chemistry (Ministry of Education), College of Chemistry, Nankai University, Tianjin 300071, China

\* Corresponding author. *E-mail:* [zyyuan@nankai.edu.cn](mailto:zyyuan@nankai.edu.cn)

## 1.1 Characterization

Powder X-ray diffraction (PXRD) patterns were collected on a Bruker D8 Focus diffractometer with Cu-K $\alpha$  irradiation. The morphologies of products were investigated by scanning electron microscopy (SEM, JEOL JSF-7500 L, 5 kV) and transmission electron microscopy (TEM, JEOL JEM-2800, 200 kV). X-ray photoelectron spectroscopy (XPS) was performed on a Thermo Scientific ESCALAB 250Xi spectrometer using a monochromatic Al K $\alpha$  X-ray (1486.6 eV) as the exciting source.

## 1.2 Electrochemical measurement

Mild electrochemical nitrogen fixation experiment was performed in a H-type reaction cell on a WaveDrive 20 Bipotentiostat/Galvanostat (Pine Research Instrumentation, USA) using a three-electrode system. The Pt, catalysts/carbon paper and Ag/AgCl rod (saturated KCl electrolyte) were used as the counter, working and reference electrodes, respectively. Calibrating all potentials according to the following equation:

$$E_{\text{RHE}} = E_{\text{Ag/AgCl}} + 0.059\text{pH} + E^{\circ}_{\text{Ag/AgCl}}$$

Before electrochemical tests, the electrolyte (0.1 M Na<sub>2</sub>SO<sub>4</sub>) was saturated with N<sub>2</sub> for 0.5 h, where N<sub>2</sub> gas ( $\geq 99.999\%$ ) passed by the alkaline solution (pH=13 KOH aqueous solution) and acid solution (pH=1 H<sub>2</sub>SO<sub>4</sub> aqueous solution) to remove any N contamination before purging into the electrolyte solution. To further ensure a pollution-free nitrogen reduction process, we pre-reduced catalysts for 3 h at -0.7 V vs. RHE under Ar to remove residual or adsorbed NO<sub>x</sub> contaminants.<sup>[1-3]</sup>

## 1.3 Determination of NH<sub>3</sub>

### 1.3.1 Analysis of ammonia by the indophenol blue method<sup>[4-6]</sup>:

Typically, 2 mL electrolyte was obtained from the cathodic reaction chamber and mixed with 2 mL NaOH solution (1 M) containing C<sub>7</sub>H<sub>5</sub>NaO<sub>3</sub> (5 wt%) and Na<sub>3</sub>C<sub>6</sub>H<sub>5</sub>O<sub>7</sub> (5 wt%), 1 mL of NaClO (0.05 M) and 0.2 mL of C<sub>5</sub>FeN<sub>6</sub>Na<sub>2</sub>O (1 wt%) for 2 h. Absorbance measurements were performed at wavelength of 655 nm. The corresponding curve ( $y = 0.4595x + 0.0068$ ,  $R^2 = 0.999$ ) showed a good linear relation between absorbance value and NH<sub>3</sub> concentration through three times independent calibrations.

### 1.3.2 Analysis of ammonia by the Nessler's reagent method:

Typically, 5 mL electrolyte was taken from the reaction cell and added into 1 mL potassium sodium tartrate ( $\text{KNaC}_4\text{H}_4\text{O}_6$ , 0.2 M) solution and 1 mL of the Nessler's reagent. Hereafter, the solution was kept to stand for 25 min for full color processing. Finally,  $\text{NH}_3$  concentration was detected using an UV-vis spectrophotometer at 420 nm wavelength. The fitting curve ( $y = 0.09x + 0.032$ ,  $R^2 = 0.999$ ) shows good linear relation of absorbance value with  $\text{NH}_3$  concentration.

### 1.3.3 Analysis of ammonia by nuclear magnetic resonance (NMR) with $^{15}\text{N}$ labelling<sup>[4-6]</sup>:

The NRR measurements were conducted using either  $^{15}\text{N}_2$  (99% isotopic purity, supplied by Beijing Yinuokai Technology Co., Ltd.) for isotopic labelling or normal  $^{14}\text{N}_2$  for comparison. Each NRR test was performed at -0.7 V (vs. RHE) for 2.5 h. Then, 0.5 mL of above solution mixed with 0.05 mL of  $d_6$ -DMSO was used for  $^1\text{H}$  nuclear magnetic resonance (NMR) spectroscopy examination (Bruker AVANCE III 600 MHz). The corresponding absolute calibration curves were obtained by using the  $^{15}\text{NH}_4\text{Cl}$  (99% isotopic purity, Shanghai Xinbo Chemical Technology Co., Ltd.) and  $^{14}\text{NH}_4\text{Cl}$  aqueous solutions with a series of known concentrations as the standards.

### 1.4 Determination of $\text{N}_2\text{H}_4$ <sup>[4-6]</sup>:

Hydrazine quantification was obtained via the Watt and Chrisp method.<sup>[4-6]</sup> Typically, 5 mL electrolyte was obtained from reaction cell and mixed with 5 mL color reagent (mixture of 5.99g  $p\text{-C}_9\text{H}_{11}\text{NO}$ , 30 mL HCl and 300 mL  $\text{C}_2\text{H}_5\text{OH}$ ) for 10 min. Absorbance measurements were performed at wavelength of 455 nm. The fitting curve ( $y = 1.1317x + 0.0199$ ,  $R^2 = 0.9997$ ) exhibited a good linear relationship between the absorbance value and  $\text{N}_2\text{H}_4$  concentration through three times independent calibrations.

### 1.5 Faradaic efficiency:

Ammonia formation rate was calculated using the following equation:

$$v_{\text{NH}_3} = \frac{V \times C_{\text{NH}_3}}{17 \times A \times t}$$

FE was calculated according to the following equation:

$$\text{FE} = \frac{3F \times n_{\text{NH}_3}}{Q}$$

Where  $V$  is the volume of the electrolyte,  $C_{\text{NH}_3}$  means  $\text{NH}_3$  concentration,  $t$  is the reduction reaction time,  $A$  is the geometric area of the cathode,  $F$  is the Faraday constant, and  $Q$  is the quantity of applied electricity.

### **1.6 Zn-N<sub>2</sub> battery tests:**

The Zn-N<sub>2</sub> battery performance tests were carried out on a homemade Zn-N<sub>2</sub> cell filled with of 0.1 M KOH, where a polished Zn plate was used as anode and carbonfiber paper supported catalyst as N<sub>2</sub> cathode. The discharge curve of Zn-N<sub>2</sub> cell was recorded on a Zahner IM6eX electrochemical workstation.

### **1.7 In situ FTIR measurement:**

The electrochemical *in situ* Fourier transform infrared (*in situ* FTIR) spectroscopy was collected using a Nexus 870 spectrometer (Nicolet) equipped with a liquid-nitrogen-cooled MCT-A detector and an EverGlo IR source. *In situ* FTIR spectra were recorded by means of time-resolved FTIR spectroscopy procedures. The resulting spectra were reported as the relative change in reflectivity and calculated as follows:

$$\frac{\Delta R}{R} = \frac{R(E_S) - R(E_R)}{R(E_R)}$$

where  $R(E_S)$  and  $R(E_R)$  are the accumulated spectra collected at sample potential  $E_S$  and reference potential  $E_R$ , respectively.

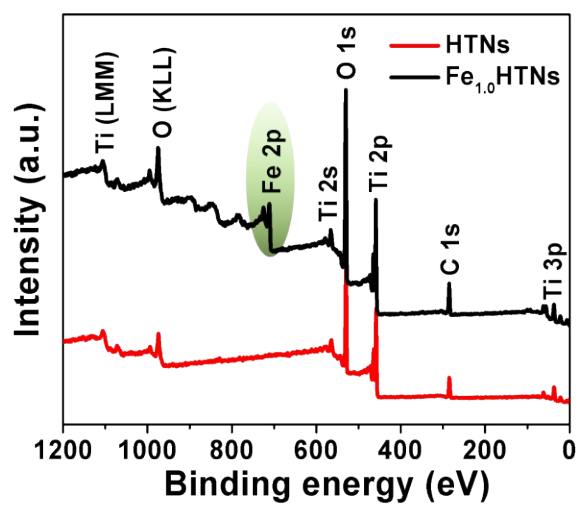


Figure S1. XPS spectra of Fe<sub>1.0</sub>HTNs and HTNs.

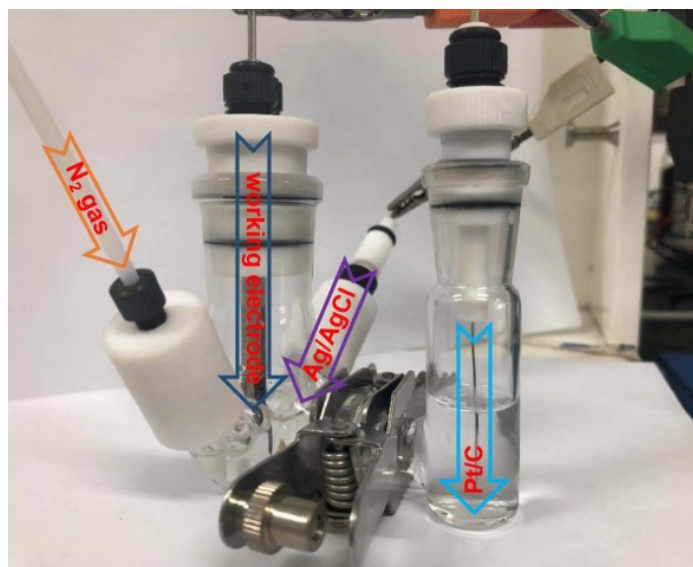
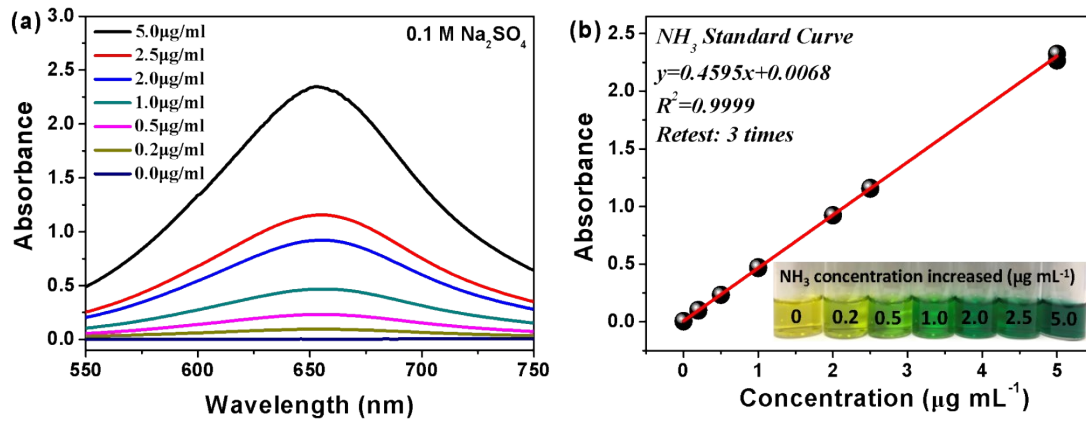
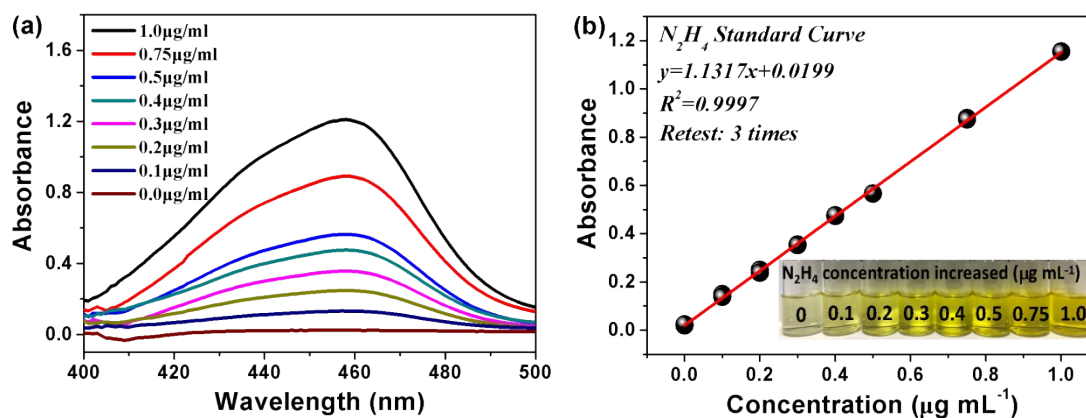


Figure S2. Representative photograph of the used H-type reaction cell for the NRR.



**Figure S3.** (a) UV-Vis absorption curves of indophenol assays with  $\text{NH}_3$  after incubated for 2 h at room temperature. (b) The corresponding calibration curve used for calculation of  $\text{NH}_3$  concentrations. All experiments were performed in 0.1 M  $\text{Na}_2\text{SO}_4$ .



**Figure S4.** (a) UV-Vis absorption curves of various  $\text{N}_2\text{H}_4$  concentrations after incubated for 20 min at room temperature. (b) The corresponding calibration curve used for estimation of  $\text{N}_2\text{H}_4$  concentrations. All experiments were performed in 0.1 M  $\text{Na}_2\text{SO}_4$ .

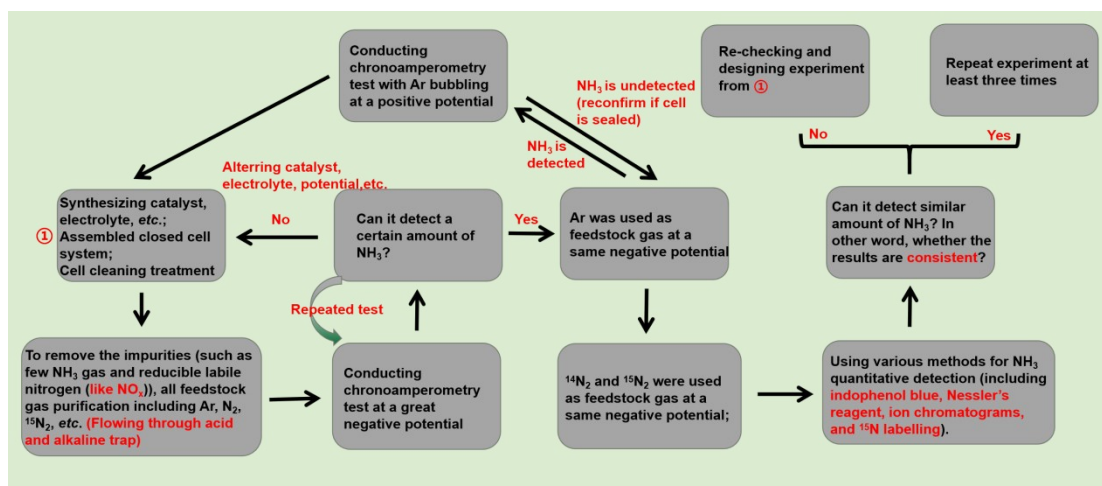


**Figure S5.** Flow diagram of control experiments to rigorously conduct NRR experiments in this work.

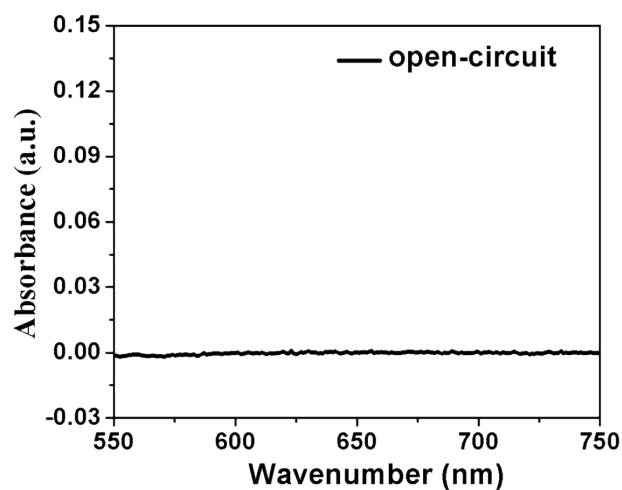


**Figure S6.** UV-visible absorption spectra of the 0.1 M  $\text{Na}_2\text{SO}_4$  electrolytes stained with indophenol indicator after charging on the  $\text{Fe}_{1.0}\text{HTNs}$  electrode at open-circuit potential for 2.5 h.

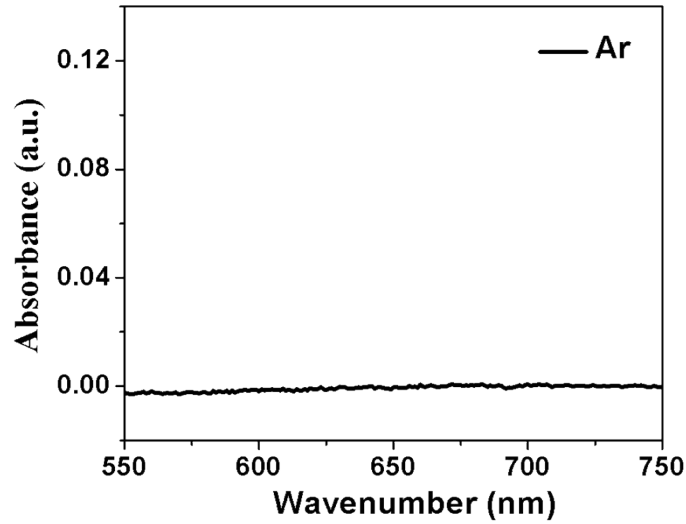


**Figure S7.** UV-visible absorption spectra of the Ar-bubbled 0.1 M  $\text{Na}_2\text{SO}_4$  electrolytes stained with indophenol indicator after charging on the  $\text{Fe}_{1.0}\text{HTNs}$  electrode at at -0.7 V vs. RHE for 2.5 h.

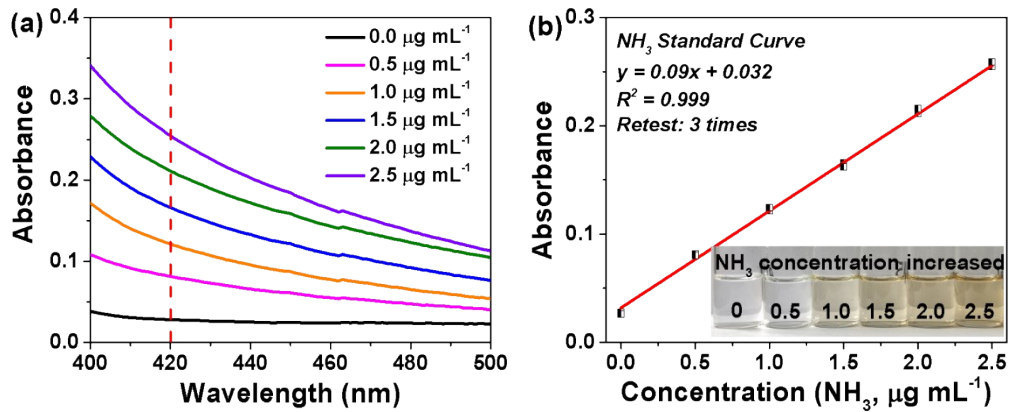


**Figure S8.** (a) UV-Vis absorption curves of Nessler's reagent assays kept with various concentrations of  $\text{NH}_3$ . (b) A calibration curve for estimating the concentrations of  $\text{NH}_3$ .

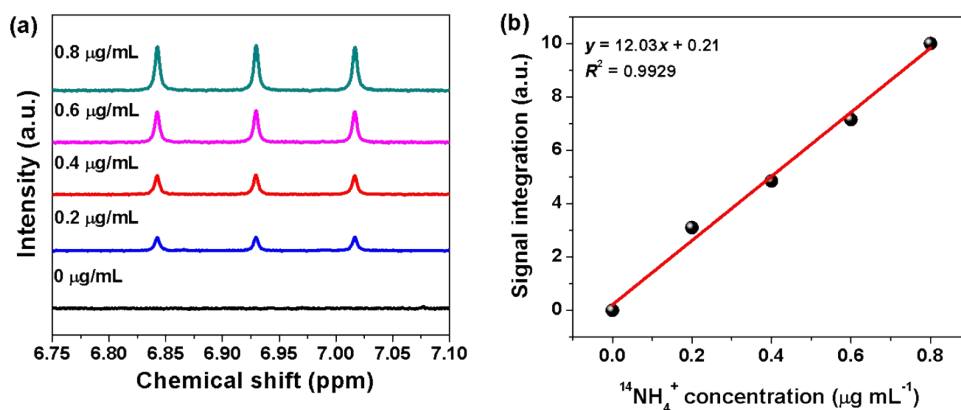


**Figure S9.** (a)  $^1\text{H}$  NMR spectra of  $^{14}\text{NH}_4^+$  standard samples with different concentrations. (b) The corresponding calibration curve of  $^{14}\text{NH}_4^+$  concentration vs. peak area intensity of NMR spectra.

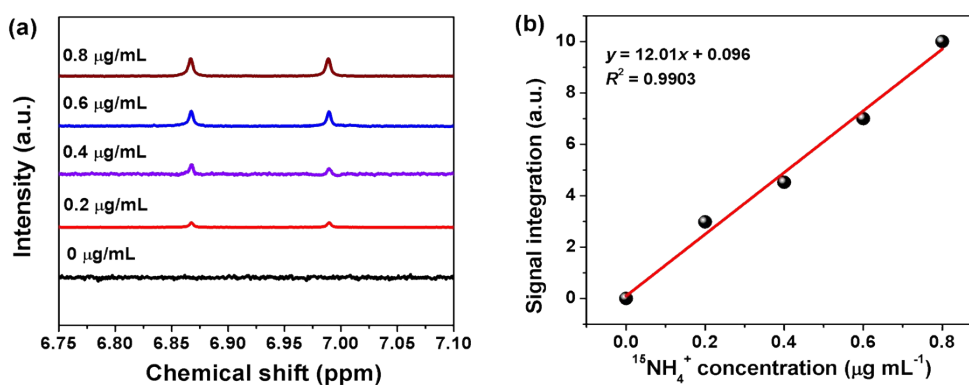


**Figure S10.** (a)  $^1\text{H}$  NMR spectra of  $^{15}\text{NH}_4^+$  standard samples with different concentrations. (b) The corresponding calibration curve of  $^{15}\text{NH}_4^+$  concentration vs. peak area intensity of NMR spectra.

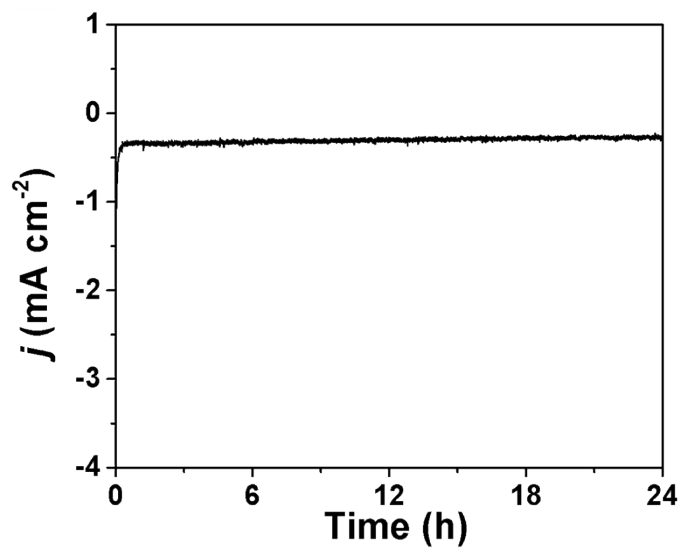


**Figure S11.** Chronoamperometry curve of Fe<sub>1.0</sub>HTNs in N<sub>2</sub>-bubbled 0.1 M Na<sub>2</sub>SO<sub>4</sub> at a fixed overpotential of -0.7 V for 24 h.

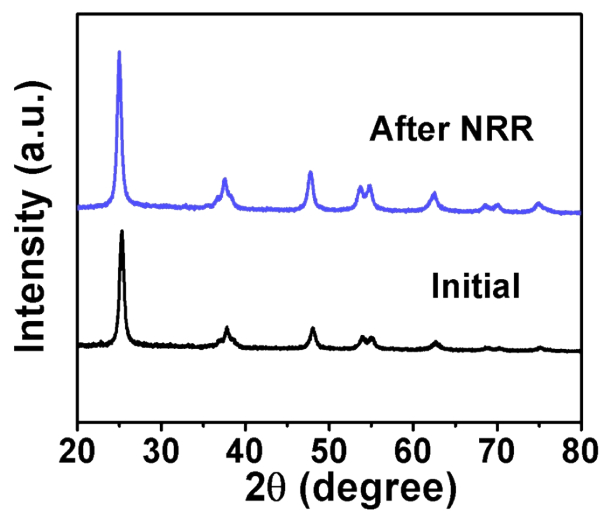


**Figure S12.** XRD patterns of Fe<sub>1.0</sub>HTNs before and after long-term NRR durability test in 0.1 M Na<sub>2</sub>SO<sub>4</sub>.

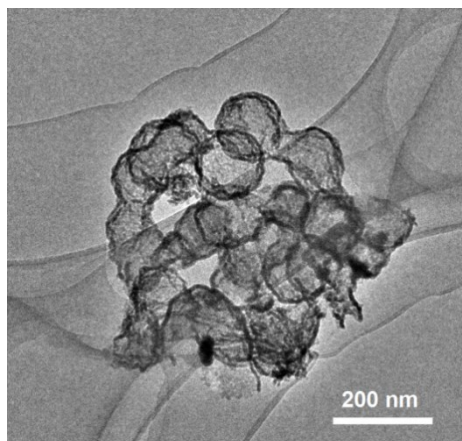


**Figure S13.** TEM image of Fe<sub>1.0</sub>HTNs after long-time NRR test in 0.1 M Na<sub>2</sub>SO<sub>4</sub>.

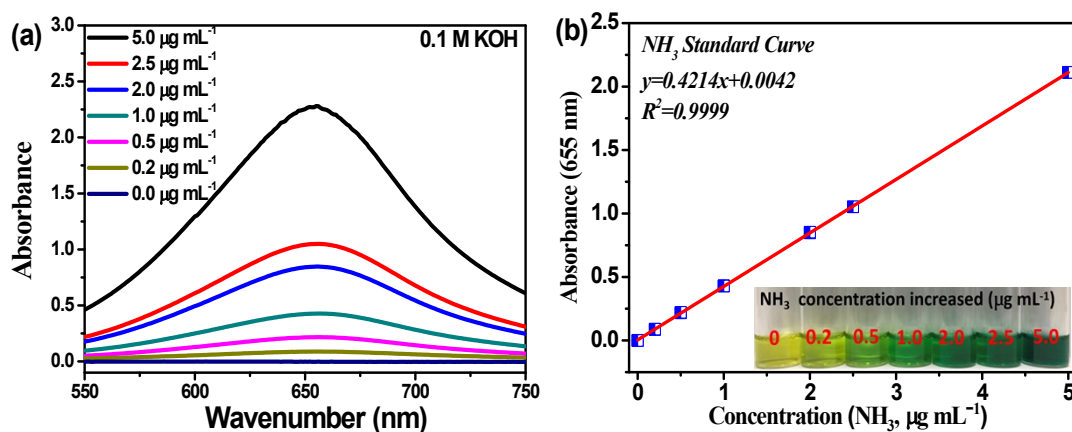


**Figure S14.** (a) UV-Vis absorption curves and (b) the corresponding calibration curve of indophenol assays with NH<sub>3</sub> after incubated for 2 h at room temperature in 0.1 M KOH.

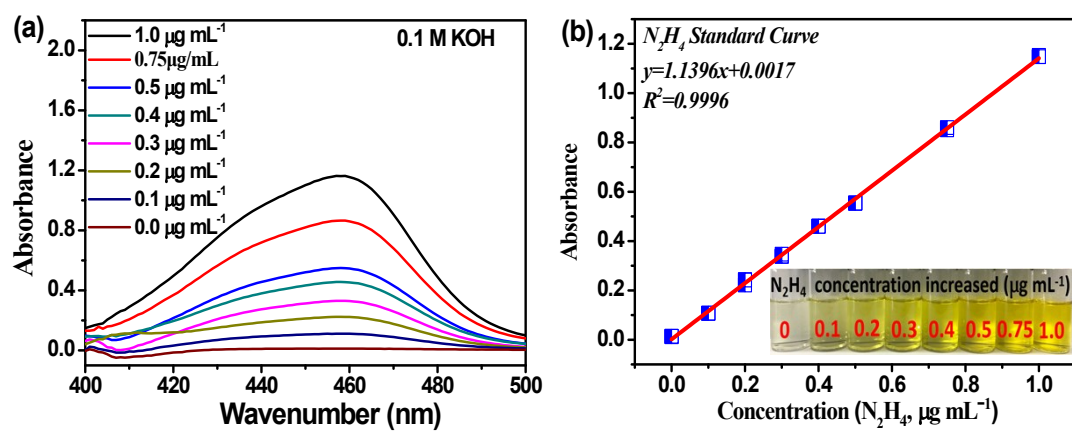


**Figure S15.** (a) UV-Vis absorption curves and (b) the corresponding calibration curve of various N<sub>2</sub>H<sub>4</sub> concentration after incubated for 30 min at room temperature in 0.1 M KOH.

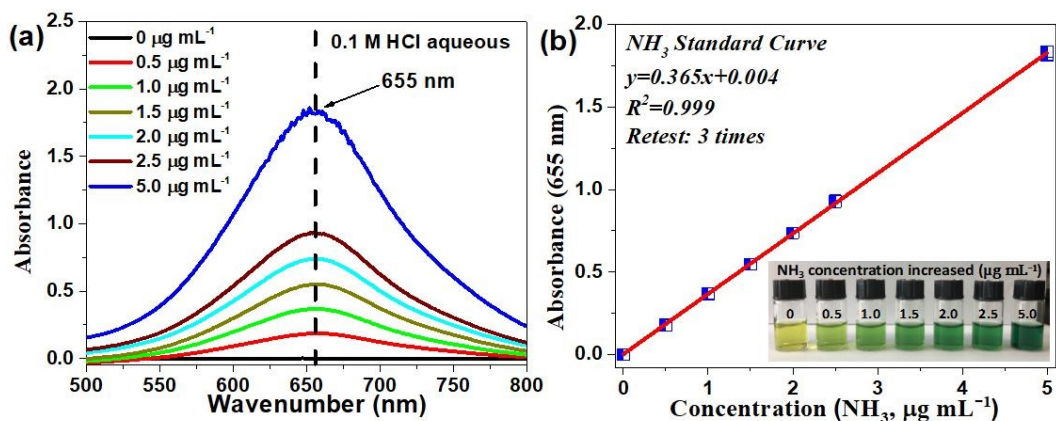


**Figure S16.** (a) UV-Vis absorption curves and (b) the corresponding calibration curve of indophenol assays with  $\text{NH}_3$  after incubated for 2 h at room temperature in 0.1 M HCl.

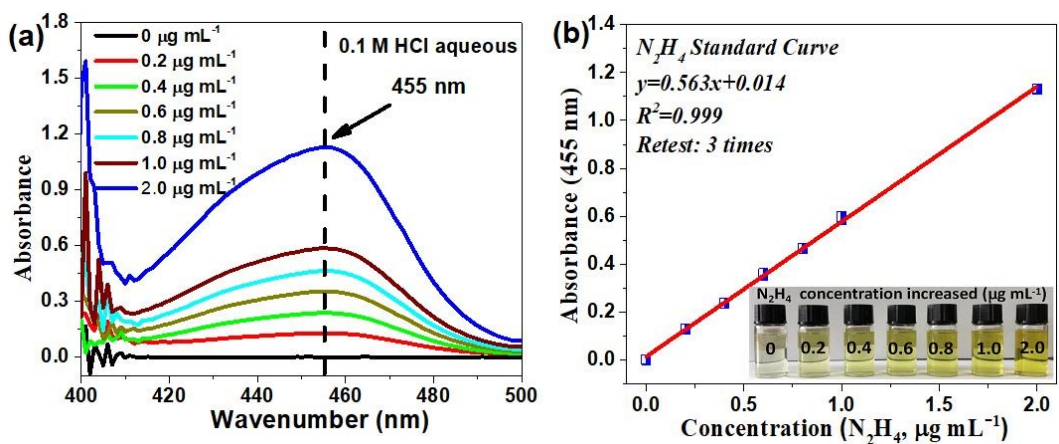


**Figure S17.** (a) UV-Vis absorption curves and (b) the corresponding calibration curve of various  $\text{N}_2\text{H}_4$  concentration after incubated for 30 min at room temperature in 0.1 M HCl.

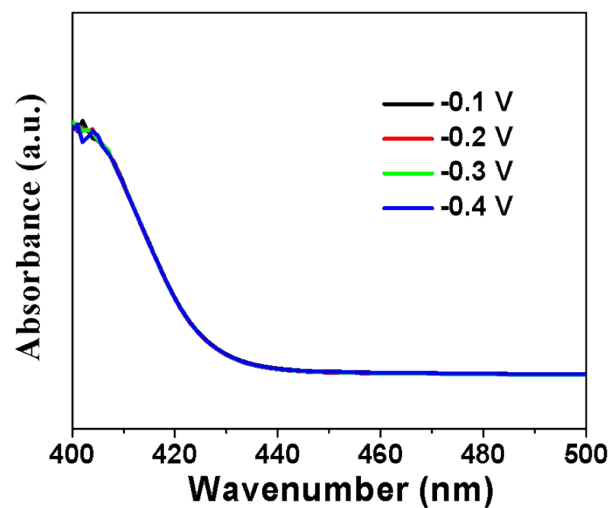


**Figure S18.** UV-Vis absorption spectra of the electrolytes (0.1 M KOH) estimated by the method of Watt and Chrisp after NRR electrolysis at different potentials.

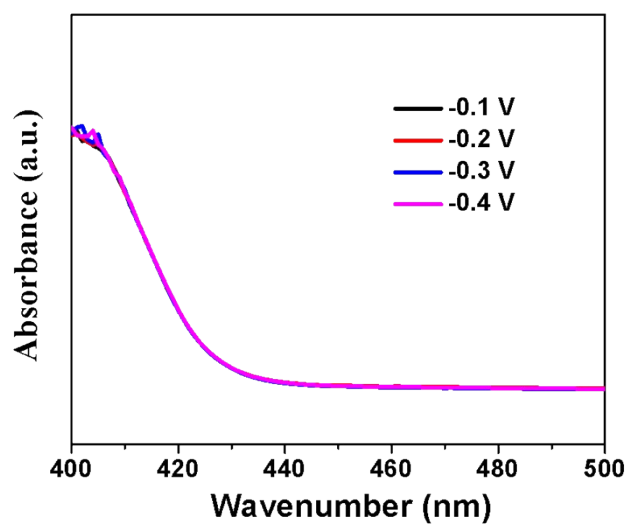


**Figure S19.** UV-Vis absorption spectra of the electrolytes (0.1 M HCl) estimated by the method of Watt and Chrisp after NRR electrolysis at different potentials.

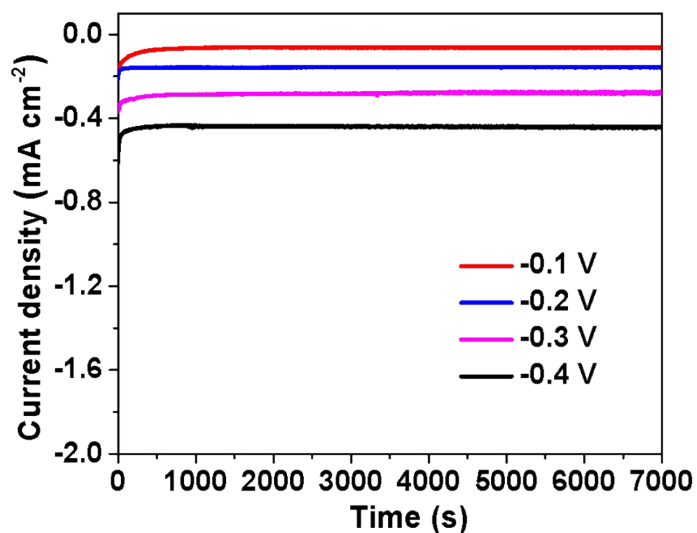


Figure S20. Chronoamperometry results of Fe<sub>1.0</sub>HTNs at each given potential in 0.1 M KOH.

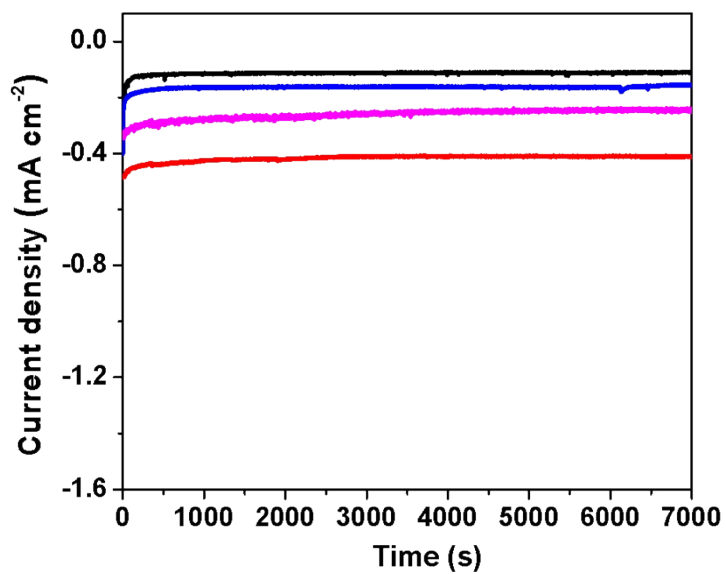
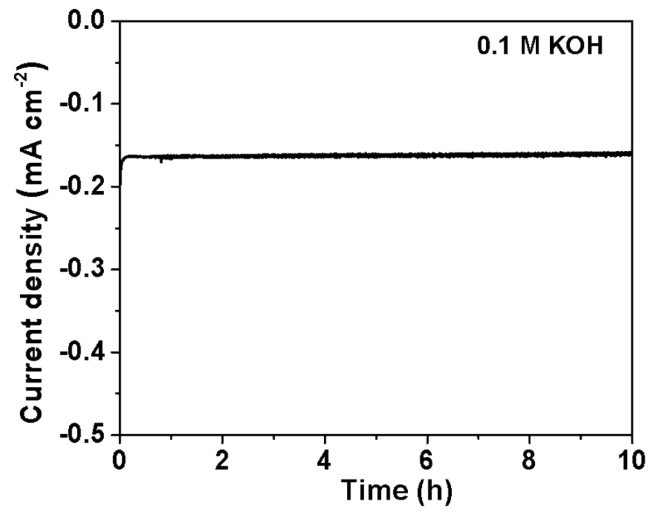
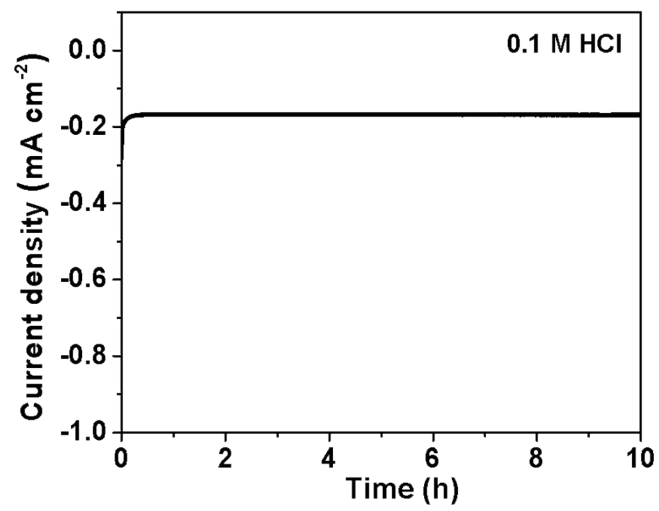


Figure S21. Chronoamperometry results of Fe<sub>1.0</sub>HTNs at each given potential in 0.1 M HCl.



**Figure S22.** Chronoamperometry curve of Fe<sub>1.0</sub>HTNs in N<sub>2</sub>-bubbled 0.1 M KOH for 10 h.



**Figure S23.** Chronoamperometry curve of Fe<sub>1.0</sub>HTNs in N<sub>2</sub>-bubbled 0.1 M HCl for 10 h.

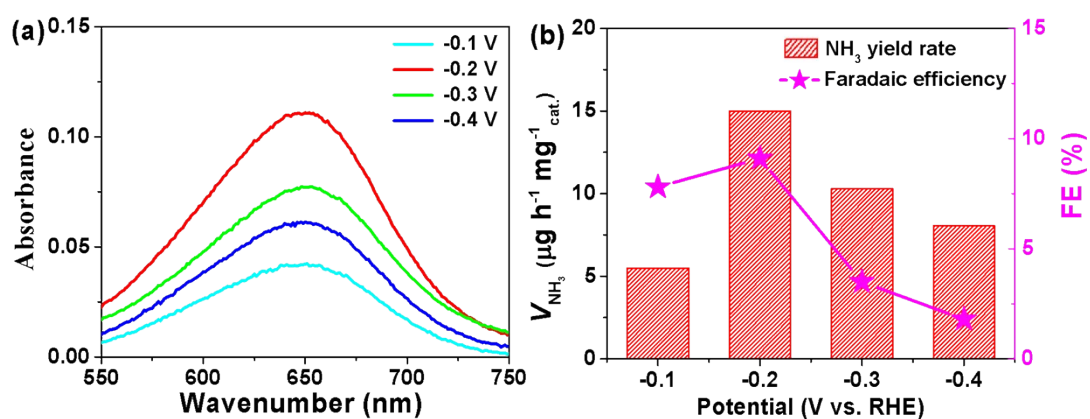


**Figure S24.** (a) UV-Vis absorption spectra of electrolytes stained with indophenol indicator under different potentials. (b) NH<sub>3</sub> yield rates and FEs for Fe<sub>1.0</sub>HTNs under different potentials in N<sub>2</sub>-bubbled 0.1 M KOH.

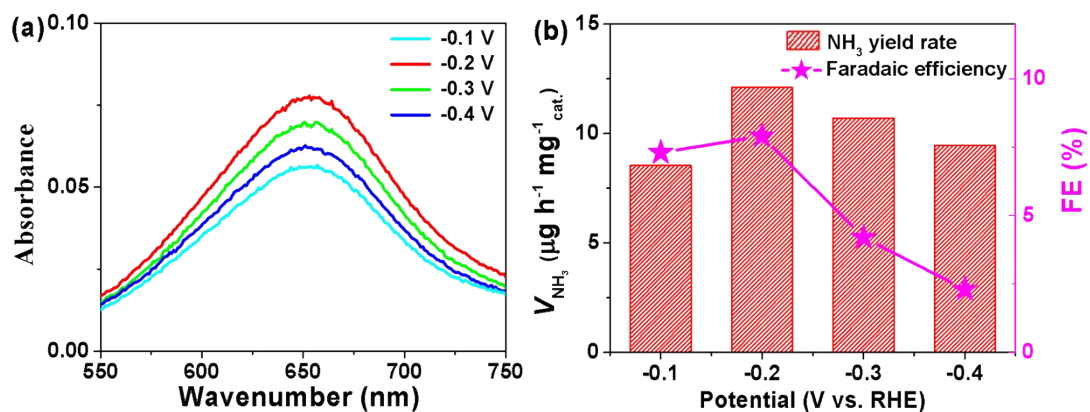


**Figure S25.** (a) UV-Vis absorption spectra of electrolytes stained with indophenol indicator under different potentials. (b) NH<sub>3</sub> yield rates and FEs for Fe<sub>1.0</sub>HTNs under different potentials in N<sub>2</sub>-bubbled 0.1 M HCl.

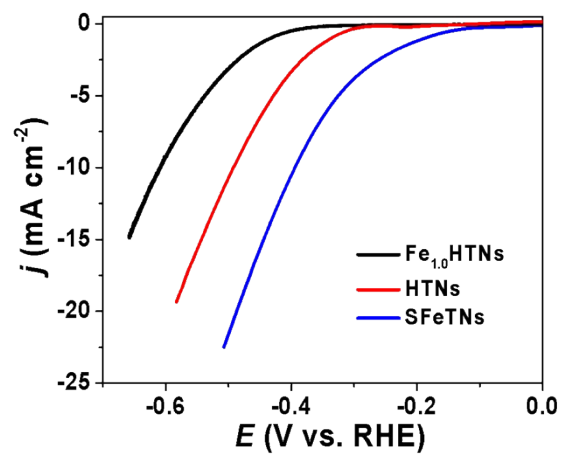


**Figure S26.** LSV curves of samples for HER obtained in Ar-saturated 0.1 M Na<sub>2</sub>SO<sub>4</sub> electrolyte.

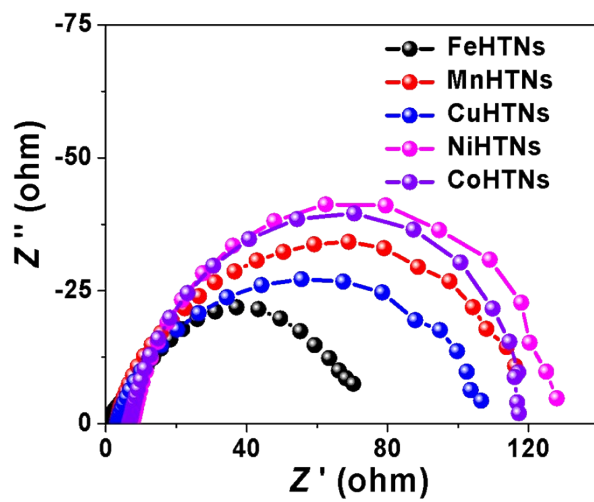


**Figure S27.** Nyquist plots of the samples on carbon paper in 0.1 M Na<sub>2</sub>SO<sub>4</sub>.

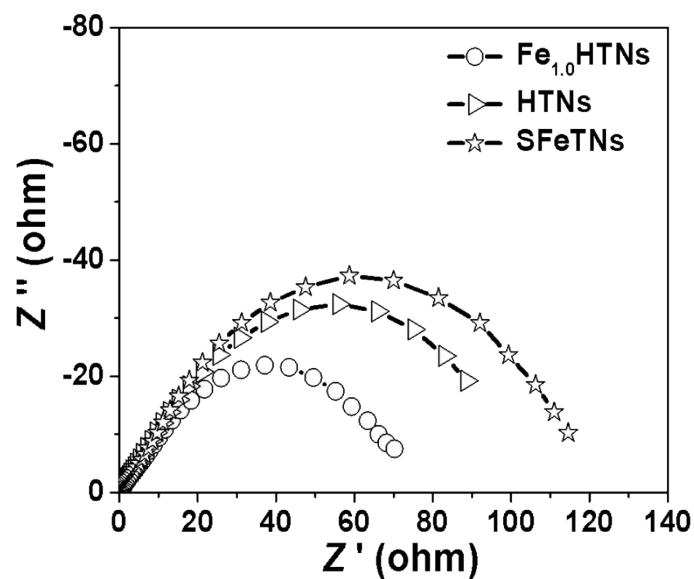


Figure S28. Nyquist plots of the samples on carbon paper in 0.1 M Na<sub>2</sub>SO<sub>4</sub>.

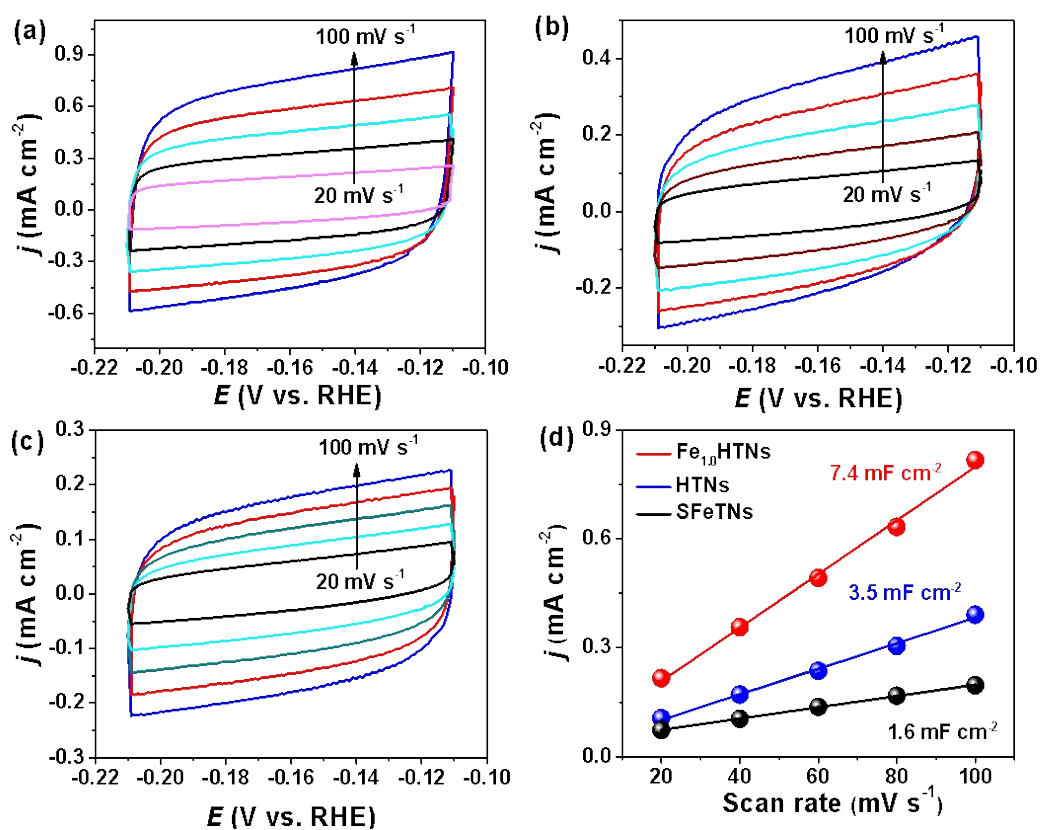
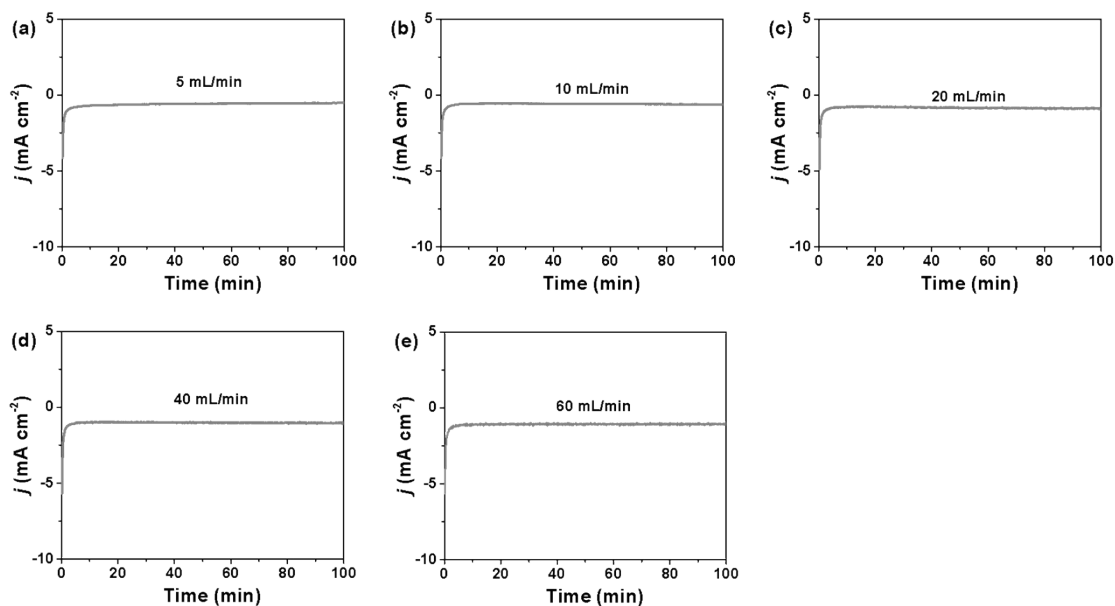
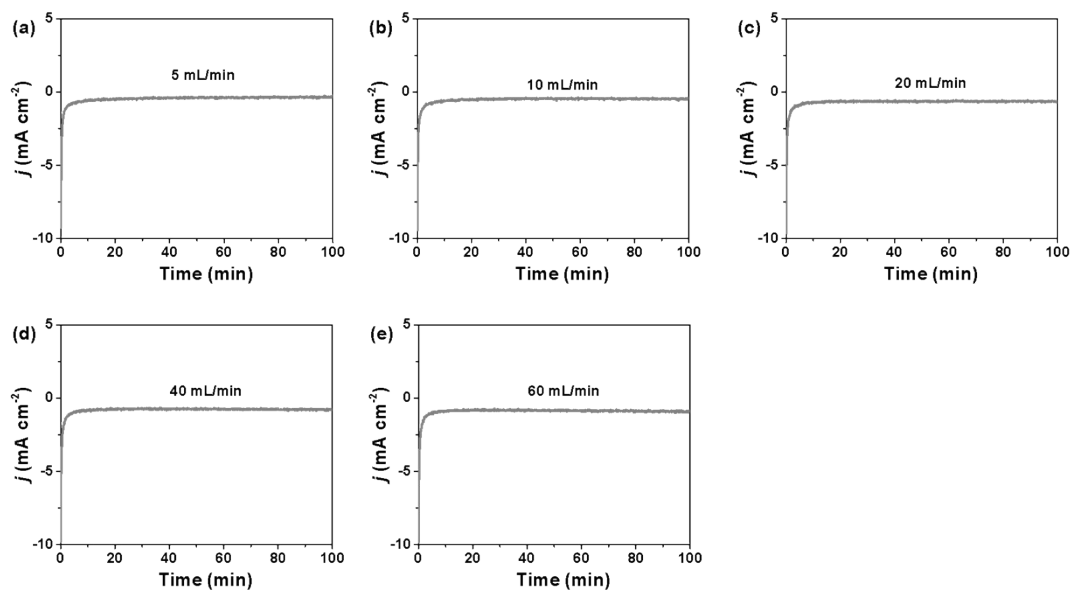


Figure S29. Cyclic voltammograms of (a) Fe<sub>1.0</sub>HTNs, (b) HTNs and (c) SFeTNs coated on carbon paper and measured at different scan rates from 20 to 100 mV s<sup>-1</sup>. (d) The corresponding plots of current density at -0.14 V versus the scan rate.



**Figure S30.** The current density of Fe<sub>1.0</sub>HTNs under different N<sub>2</sub> flow rates: (a) 5 mL/min, (b) 10 mL/min, (c) 20 mL/min, (d) 40 mL/min and (e) 60 mL/min.



**Figure S31.** The current density of SFeTNs under different N<sub>2</sub> flow rates: (a) 5 mL/min, (b) 10 mL/min, (c) 20 mL/min, (d) 40 mL/min and (e) 60 mL/min.

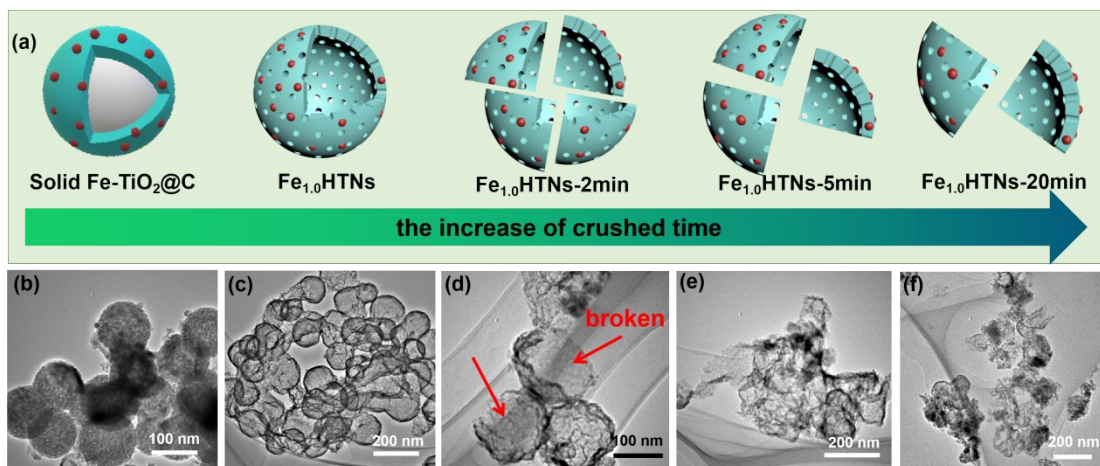


**Figure S32.** Schematic illustration of solid Fe-TiO<sub>2</sub>@C precursor, Fe<sub>1.0</sub>HTNs, and crushed Fe<sub>1.0</sub>HTNs-*t* samples (*t* represents the crushed time). (b-f) The corresponding TEM images of solid Fe-TiO<sub>2</sub>@C, Fe<sub>1.0</sub>HTNs, Fe<sub>1.0</sub>HTNs-2min, Fe<sub>1.0</sub>HTNs-5min, and Fe<sub>1.0</sub>HTNs-20min.

The solid Fe-TiO<sub>2</sub>@C sphere precursor with a size of ~100 nm (**Figure S32b**) was carbonized in air to form Fe<sub>1.0</sub>HTNs hollow nanospheres (**Figure 32c**). Then, Fe<sub>1.0</sub>HTNs hollow nanospheres were further crushed mechanically by a static pressure of ~32 MPa with the increase over time from 2 min to 20 min (**Figure 32d-f**). The integrity of the spherical shell was gradually destroyed. Herein, the synthesis method used was based on the previous literatures with a minor modification. [*J. Am. Ceram. Soc.*, 2014, 97.2: 407-412; *J. Alloy. Compd.* 2018, 769, 521-531; *J. Mol. Catal. A: Chem.* 2005, 226, 93-100; *J. Am. Chem. Soc.* 2007, 129, 8406-8407].

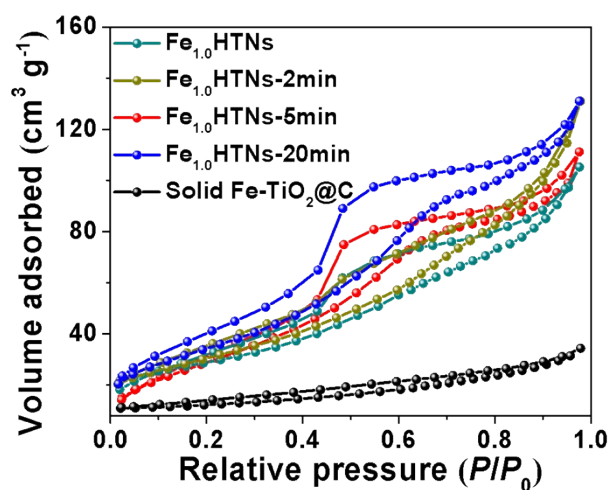


**Figure S33.** N<sub>2</sub> adsorption-desorption isotherm curves for various samples.

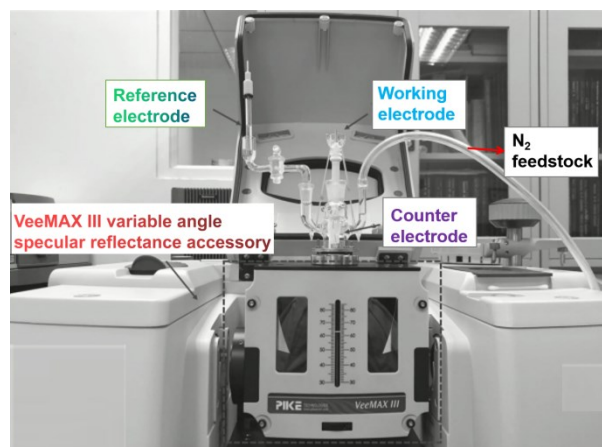


**Figure S34.** Representative picture of *in situ*-FTIR spectroscopy testing device with Nicolet iS50 spectrometer equipped with VeeMAX III variable angle specular reflectance accessory and an electrochemical reaction cell with a  $\text{CaF}_2$  bottom.

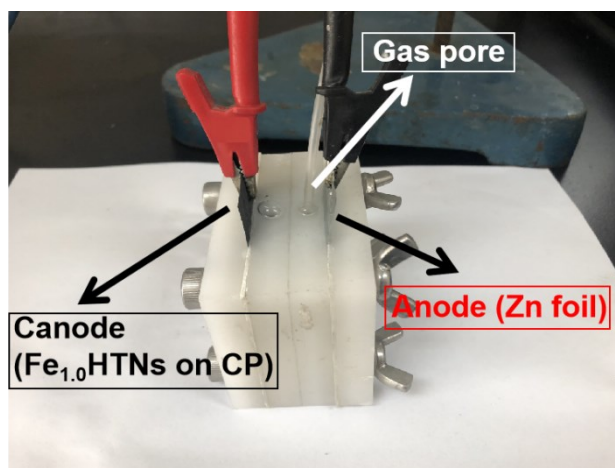


**Figure S35.** The photograph of Zn-N<sub>2</sub> battery.

**Table S1.** Comparison of NRR activity of some recently reported electrocatalysts in 0.1 M Na<sub>2</sub>SO<sub>4</sub>.

Catalyst	Electrolyte	NH <sub>3</sub> yield ( $\mu\text{g h}^{-1} \text{mg}^{-1}_{\text{cat.}}$ )	FE (%)	Ref.
Fe <sub>1.0</sub> HTNs	0.1 M Na <sub>2</sub> SO <sub>4</sub>	43.14	16.35	This work.
Fe <sub>1.0</sub> HTNs	0.1 M KOH	15.2	9.1	This work.
Fe <sub>1.0</sub> HTNs	0.1 M HCl	12.1	7.9	This work.
Ag <sub>3</sub> Cu BPNs	0.1 M Na <sub>2</sub> SO <sub>4</sub>	24.59	13.28	7
PdCuIr-LS	0.1 M Na <sub>2</sub> SO <sub>4</sub>	13.43	5.29	8
V <sub>2</sub> O <sub>3</sub> /C	0.1 M Na <sub>2</sub> SO <sub>4</sub>	12.3	7.28	9
VO <sub>2</sub> /CP	0.1 M Na <sub>2</sub> SO <sub>4</sub>	14.85	3.97	10
TiO <sub>2</sub> -rGO	0.1 M Na <sub>2</sub> SO <sub>4</sub>	15.13	3.3	11
Mn <sub>3</sub> O <sub>4</sub> nanocubes	0.1 M Na <sub>2</sub> SO <sub>4</sub>	11.6	3.0	12
Cr <sub>2</sub> O <sub>3</sub> microspheres	0.1 M Na <sub>2</sub> SO <sub>4</sub>	25.3	6.78	13
CoO	0.1 M Na <sub>2</sub> SO <sub>4</sub>	21.5	8.3	14
VO <sub>2</sub> hollow microspheres	0.1 M Na <sub>2</sub> SO <sub>4</sub>	14.85	3.97	15
CeO <sub>2</sub> nanorod	0.1 M Na <sub>2</sub> SO <sub>4</sub>	16.4	3.7	16
NiO/G	0.1 M Na <sub>2</sub> SO <sub>4</sub>	18.6	7.8	17
La <sub>2</sub> O <sub>3</sub>	0.1 M Na <sub>2</sub> SO <sub>4</sub>	17.04	4.76	18
MoS <sub>2</sub> nanoflower	0.1 M Na <sub>2</sub> SO <sub>4</sub>	29.28	8.34	19
S-CNS	0.1 M Na <sub>2</sub> SO <sub>4</sub>	19.07	7.47	20
d-FG	0.1 M Na <sub>2</sub> SO <sub>4</sub>	9.3	4.2	21
BNS	0.1 M Na <sub>2</sub> SO <sub>4</sub>	13.22	4.04	22
MBN	0.1 M Na <sub>2</sub> SO <sub>4</sub>	18.2	5.5	23

## References

- (1) Liu, H.; Zhang, Y.; Luo, J. The removal of inevitable NO species in catalysts and the selection of appropriate membrane for measuring electrocatalytic ammonia synthesis accurately. *J. Energy Chem.* **2020**, *49*, 51-58.
- (2) Chen, G. F.; Ren, S.; Zhang, L.; Cheng, H.; Luo, Y.; Zhu, K.; Ding, L. X.; Wang, H. Advances in Electrocatalytic N<sub>2</sub> Reduction-Strategies to Tackle the Selectivity Challenge. *Small Methods* **2018**, *3* (6), 1800337.
- (3) Zheng, J.; Lyu, Y.; Qiao, M.; Veder, J. P.; Marco, R. D.; Bradley, J.; Wang, R.; Li, Y.; Huang, A.; Jiang, S. P.; Wang, S. Tuning the Electron Localization of Gold Enables the Control of Nitrogen-to-Ammonia Fixation. *Angew. Chem. Int. Ed.* **2019**, *58* (51), 18604-18609.
- (4) Lv, X.-W.; Wang, L.; Wang, G.; Hao, R.; Ren, J.-T.; Liu, X.; Duchesne, P. N.; Liu, Y.; Li, W.; Yuan, Z.-Y. ZIF-supported AuCu nanoalloy for ammonia electrosynthesis from nitrogen and thin air. *J. Mater. Chem. A* **2020**, *8* (18), 8868-8874.
- (5) Lv, X.-W.; Liu, Y.; Hao, R.; Tian, W.; Yuan, Z.-Y. Urchin-like Al-Doped Co<sub>3</sub>O<sub>4</sub> Nanospheres Rich in Surface Oxygen Vacancies Enable Efficient Ammonia Electrosynthesis. *ACS Appl. Mater. Interfaces* **2020**, *12* (15), 17502-17508.
- (6) Lv, X.-W.; Liu, Y.; Wang, Y.-S.; Liu, X.-L.; Yuan, Z.-Y. Encapsulating vanadium nitride nanodots into N, S-codoped graphitized carbon for synergistic electrocatalytic nitrogen reduction and aqueous Zn-N<sub>2</sub> battery. *Appl. Catal. B: Environ.* **2020**, 119434.
- (7) Yu, H.; Wang, Z.; Yang, D.; Qian, X.; Xu, Y.; Li, X.; Wang, H.; Wang, L. Bimetallic Ag<sub>3</sub>Cu porous networks for ambient electrolysis of nitrogen to ammonia. *J. Mater. Chem. A* **2019**, *7* (20), 12526-12531.
- (8) Kumar, R. D.; Wang, Z.; Li, C.; Kumar, A. V. N.; Xue, H.; Xu, Y.; Li, X.; Wang, L.; Wang, H. Trimetallic PdCuIr with long-spined sea-urchin-like morphology for ambient electroreduction of nitrogen to ammonia. *J. Mater. Chem. A* **2019**, *7* (7), 3190-3196.
- (9) Zhang, R.; Han, J.; Zheng, B.; Shi, X.; Asiri, A. M.; Sun, X. Metal-organic framework-derived shuttle-like V<sub>2</sub>O<sub>3</sub>/C for electrocatalytic N<sub>2</sub> reduction under ambient conditions. *Inorg. Chem. Front.* **2019**, *6* (2), 391-395.
- (10) Zhang, R.; Guo, H.; Yang, L.; Wang, Y.; Niu, Z.; Huang, H.; Chen, H.; Xia, L.; Li, T.; Shi, X. Electrocatalytic N<sub>2</sub> Fixation over Hollow VO<sub>2</sub> Microspheres at Ambient Conditions. *ChemElectroChem* **2019**, *6* (4), 1014-1018.
- (11) Zhang, X.; Liu, Q.; Shi, X.; Asiri, A. M.; Luo, Y.; Sun, X.; Li, T. TiO<sub>2</sub> nanoparticles-reduced graphene oxide hybrid: an efficient and durable electrocatalyst toward artificial N<sub>2</sub> fixation to NH<sub>3</sub> under ambient conditions. *J. Mater. Chem. A* **2018**, *6* (36), 17303-17306.
- (12) Wu, X.; Xia, L.; Wang, Y.; Lu, W.; Liu, Q.; Shi, X.; Sun, X. Mn<sub>3</sub>O<sub>4</sub> Nanocube: An Efficient Electrocatalyst Toward Artificial N<sub>2</sub> Fixation to NH<sub>3</sub>. *Small* **2018**, *14* (48), 1803111.
- (13) Zhang, Y.; Qiu, W.; Ma, Y.; Luo, Y.; Tian, Z.; Cui, G.; Xie, F.; Chen, L.; Li, T.; Sun, X. High-performance electrohydrogenation of N<sub>2</sub> to NH<sub>3</sub> catalyzed by multishelled hollow Cr<sub>2</sub>O<sub>3</sub> microspheres under ambient conditions. *ACS Catal.* **2018**, *8* (9), 8540-8544.
- (14) Chu, K.; Liu, Y.-p.; Li, Y.-b.; Zhang, H.; Tian, Y. Efficient electrocatalytic N<sub>2</sub> reduction on CoO quantum dots. *J. Mater. Chem. A* **2019**, *7* (9), 4389-4394.
- (15) Zhang, R.; Guo, H.; Yang, L.; Wang, Y.; Niu, Z.; Huang, H.; Chen, H.; Xia, L.; Li, T.; Shi, X. Electrocatalytic N<sub>2</sub> Fixation over Hollow VO<sub>2</sub> Microspheres at Ambient Conditions. *ChemElectroChem*

**2019**, 6 (4), 1014-1018.

(16) Xu, B.; Xia, L.; Zhou, F.; Zhao, R.; Chen, H.; Wang, T.; Zhou, Q.; Liu, Q.; Cui, G.; Xiong, X. Enhancing Electrocatalytic N<sub>2</sub> Reduction to NH<sub>3</sub> by CeO<sub>2</sub> Nanorod with Oxygen Vacancies. *ACS sustain. Chem. Eng.* **2019**, 7 (3), 2889-2893.

(17) Chu, K.; Liu, Y.-p.; Wang, J.; Zhang, H. NiO Nanodots on Graphene for Efficient Electrochemical N<sub>2</sub> Reduction to NH<sub>3</sub>. *ACS Appl. Energy Mater.* **2019**, 2 (3), 2288–2295.

(18) Xu, B.; Liu, Z.; Qiu, W.; Liu, Q.; Sun, X.; Cui, G.; Wu, Y.; Xiong, X. La<sub>2</sub>O<sub>3</sub> nanoplate: An efficient electrocatalyst for artificial N<sub>2</sub> fixation to NH<sub>3</sub> with excellent selectivity at ambient condition. *Electrochim. Acta* **2019**, 298, 106-111.

(19) Li, X.; Li, T.; Ma, Y.; Wei, Q.; Qiu, W.; Guo, H.; Shi, X.; Zhang, P.; Asiri, A. M.; Chen, L. Boosted Electrocatalytic N<sub>2</sub> Reduction to NH<sub>3</sub> by Defect-Rich MoS<sub>2</sub> Nanoflower. *Adv. Energy Mater.* **2018**, 8 (30), 1801357.

(20) Xia, L.; Wu, X.; Wang, Y.; Niu, Z.; Liu, Q.; Li, T.; Shi, X.; Asiri, A. M.; Sun, X. S-Doped Carbon Nanospheres: An Efficient Electrocatalyst toward Artificial N<sub>2</sub> Fixation to NH<sub>3</sub>. *Small Methods* **2018**, 1800251.

(21) Zhao, J.; Yang, J.; Ji, L.; Wang, H.; Chen, H.; Niu, Z.; Liu, Q.; Li, T.; Cui, G.; Sun, X. Defect-rich fluorographene nanosheets for artificial N<sub>2</sub> fixation under ambient conditions. *Chem. Commun.* **2019**, 55, 4266-4269.

(22) Zhang, X.; Wu, T.; Wang, H.; Zhao, R.; Chen, H.; Wang, T.; Wei, P.; Luo, Y.; Zhang, Y.; Sun, X. Boron Nanosheet: An Elemental Two-Dimensional (2D) Material for Ambient Electrocatalytic N<sub>2</sub>-to-NH<sub>3</sub> Fixation in Neutral Media. *ACS Catal.* **2019**, 9, 4609-4615.

(23) Zhao, J.; Ren, X.; Li, X.; Fan, D.; Sun, X.; Ma, H.; Wei, Q.; Wu, D. High-performance N<sub>2</sub>-to-NH<sub>3</sub> fixation by a metal-free electrocatalyst. *Nanoscale* **2019**, 11 (10), 4231-4235.